ATL-PHYS-2002-004
07/02/2002

Isolation of Photons

M. Wielers
TRIUMF, Vancouver, Canada

Abstract

Photon identification in ATLAS is based on the shower shapes in the calorimeters, conversion reconstruction and a track veto. In this note the additional γ/jet separation power is evaluated if isolation is required around the shower as additional criteria. This study has been done for prompt photons and photons from $H \rightarrow \gamma\gamma$ decays. Both types of photons are generally well isolated. For isolation different approaches have been compared which led to a similar final γ/jet separation power. Using isolation as additional criteria for photon identification and requiring that at least 99% of the photons survive the 'standard' photon identification cuts, a jet rejection of $2470 \pm 240 (1030 \pm 70)$ has been found for prompt photons at $E_T \approx 20$ GeV at low (design) luminosity. Compared to the 'standard' photon identification, this corresponds to an improvement in jet rejection of 70% (15%). For photons from Higgs decays the jet rejection could be improved by 40% (10-20%) at low (design) luminosity at $E_T \approx 20$ GeV for a 80% photon efficiency. These numbers have been obtained for an optimisation of the 'standard' photon identification cuts and the isolation cuts at the same time.

1 Introduction

At LHC an excellent photon identification is mandatory for the search of a possible Standard Model Higgs boson in the mass range up to 130 GeV. Combining the results of the four LEP experiments a lower limit of the Higgs mass of 114.1 GeV at a 95% confidence level is obtained. The likelihood analysis shows a preference for a Higgs boson with a mass of 115.6 GeV [1]. A good photon reconstruction is as well needed to measure prompt photons in order to obtain information on the gluon density.

In this note, isolation of photons is studied for prompt photons and photons from Higgs decays and its impact on photon identification is evaluated. In previous studies photon identification is 'only' based on the analysis of the shower shape in the electromagnetic calorimeter, leakage into the hadronic calorimeter, conversions identification in the inner detector and a track veto. Thus, only the shower core is analysed so far and no 'direct' use of isolation around the shower in the calorimeters is required besides the 'loose' isolation cuts applied on the first level trigger. One aim of this study is to compare different isolation methods. There is the fixed cone method which is looking at the energy deposit in an isolation ring around the shower. In another approach the transverse energy in isolation rings with different outer radii are compared. This second approach is favoured by theory.

The outline of this note is as follows. The next section gives an overview of the datasets used in this study. After a short review of the 'standard' photon identification criteria, the different photon isolation approaches are discussed in section 4. Section 5 shows the estimated improvement in γ/jet separation using the different isolation methods in addition to the 'standard' photon identification cuts for QCD prompt photons. A similar study for photons from Higgs decays will be presented in section 6. In the last section the main results are summarised.

2 Data samples

The detector layout used for this study corresponds to the detector design as described in [2] and [3]. In ATLAS photons can be reconstructed in the rapidity region $|\eta| < 2.5$. To study γ/jet separation single photons with different transverse energies (20, 40, and 60 GeV) produced in this rapidity region have been generated and were fully simulated with GEANT [6] using DICE 98_2 as detector simulation. These are typical photon energies of photons from $H \rightarrow \gamma\gamma$ decays. Very high energetic photons have not been considered for two reasons. At very high energies the cross section of the jet background is much lower and gamma/jet seperation becomes less of an issue. Looking at the gamma/jet separation power as a function of E_T, at $E_T \approx 60$ GeV saturation is reached and no further improvement in jet rejection is expected. For very high energetic photons and jets no simulations are so far available. This is mainly due to the time of producing high energetic particles with Geant. These single photon events are by definition isolated and therefore isolation needs to be rechecked within the 'real' physics environment. Isolation is dependent on the physics process considered and will be studied in this note for photons from $H \rightarrow \gamma\gamma$ decays and QCD prompt photons. For prompt photon events only the 'few' events found in the jet sample which is described in the next paragraph are available. For photons from Higgs decays 10000 Higgs events with $m(H) = 100$ GeV are used. The events are generated by PYTHIA 5.7 [7] in the rapidity range $|\eta| < 2.5$ and are fully simulated using DICE 98_2. For the reconstruction of Higgs

events, the events have to pass the following kinematical cuts to obtain a good ratio of signal to background:

- at least two electromagnetic clusters are found. One cluster has to exceed $E_T > 40$ GeV and the other $E_T > 25$ GeV
- both clusters are within $|\eta| < 2.5$

In addition, the following fiducial area cuts in the electromagnetic calorimeter are applied for precision physics:

- events with one of the two photon showers in the transition region between the barrel end electromagnetic end-cap calorimeter ($1.37 < |\eta| < 1.52$) are rejected.
- both clusters are within $|\eta| < 2.47$. Due to the change in granularity at $|\eta| = 2.5$ the variables used for γ/jet separation as well as η cannot be precisely calculated above this value.
- the variables used for γ/jet separation using the first sampling are considered in $|\eta| < 1.37$ and $1.52 < |\eta| < 2.37$.

For the study of photon identification two sets of around one million fully simulated QCD dijet events each were used. On parton level each jet was required to have a p_T of at least 17 (35) GeV and a rapidity within ± 2.7. In the following, these jets will be referred to as low and high-E_T jet sample. The events were generated with Pythia 5.7. For the detector simulation the DICE 96_12 geometry was used for low-E_T sample and the DICE 98_2 geometry for the high-E_T sample (see [8] for the differences between these two geometries). Initial as well as final state radiation was simulated. In addition to QCD dijet events, other physics processes such as prompt photon events, intermediate W and Z production, and top production were generated according to their cross sections. Events which would not pass trigger LVL1 are immediately rejected before being processed by GEANT. To obtain manageable datasets the QCD-dijets are required to pass the pseudo LVL1 trigger conditions for the electron stream using ATRIG [9]. The selection criteria are looser than those for trigger LVL1 and are described in [10] and [8]. After this trigger level only 2 (2)% of the total number of all QCD events generated for the low (high)-E_T sample survive at low luminosity. These events are further processed by the actual LVL1 trigger [8].

The LVL1 electron/photon trigger includes two trigger menu item. There is the single object trigger EM20i (EM30i) which is efficient for electrons and photons with $E_T \geq 20$ (30) GeV and the double-object trigger EM15i×2 (EM20i×2) requiring two candidates having $E_T \geq 15$ (20) GeV at low (high) luminosity. For the studies presented here the double-object trigger was changed in a single-object trigger to study 20 GeV photons. The LVL1 selection criteria are explained in [8].

At low luminosity, the calorimeter response is simulated including electronic noise. To reduce this noise digital filtering is applied. At high luminosity, the default electronic shaping is assumed. Pileup was added in the calorimeters and the inner detector. For the trigger studies ATRIG is used and for the offline analysis ATRECON [12, 13]. In the following low luminosity refers to $L = 10^{33} cm^{-2} s^{-1}$ and high luminosity to $L = 10^{34} cm^{-2} s^{-1}$.

3 Photon Identification

Jets and photons can be separated by the analysis of the leakage of electromagnetic showers into the hadronic calorimeter and the study of the shower shapes in the first and second samplings of the electromagnetic calorimeters. This analysis is done in the region around the shower direction of ($\Delta\eta \times \Delta\phi = 0.2 \times 0.2, 0.175 \times 0.175, 0.125 \times 0.2$ in the first sampling of the hadronic calorimeter and the second and first sampling of the em calorimeters respectively. It should be noted that this region is larger than a 'typical' cluster size of $\Delta\eta \times \Delta\phi = 0.075 \times 0.125$ for unconverted photons. The following criteria are used for γ/jet separation using the calorimeter information:

- Isolation in the hadronic calorimeter. To measure the leakage, the transverse energy in the first sampling of the hadronic calorimeter is calculated in a window of size $\Delta\eta \times \Delta\phi = 0.2 \times 0.2$. The leakage scales with $1/E_T$.

- shower shape in η direction in the second em sampling ($E_2(3 \times 7)/E_2(7 \times 7)$). Photons and electrons deposit most of their energy in 3×7 cells.

- shower shape in ϕ direction in the second em sampling ($E_2(3 \times 3)/E_2(3 \times 7)$). Analogue to the isolation in η direction the ratio of the energy deposited in 3×3 cells divided by the energy summed in 3×7 cells is considered. In this direction the isolation is less good due to converted photons. A cut on $E_2(3 \times 3)/E_2(3 \times 7)$ is therefore more sensitive to converted than unconverted photons.

- shower width in η direction in the second em layer ($\omega_{\eta 2}$). The shower width is calculated in 3×5 cells using the energy weighted sum over all cells ($\omega_{\eta 2} = \sqrt{\sum E_c \cdot \eta^2 / \sum E_c - (\sum E_c \cdot \eta / \sum E_c)^2}$). This width depends on the particle impact point inside the cell. This dependance of the width with respect to the position within the cell is unfolded and is normalised to correspond to the impact point of the shower in the centre of the cell.

- Search for a second maximum using the strip information of the first em layer. The energy deposit in a window $\Delta\eta \times \Delta\phi = 0.125 \times 0.2$ is examined. Two ϕ-bins are summed and the shower in η-direction is scanned for a second maximum. In case more than two maxima are found the second highest maxima is considered. To be stable against fluctuations the energy of the strip where a second maximum is located has to exceed a value which depends linearly on the E_T of the electromagnetic cluster. In addition, the difference of the energy in the strip with the second maximum and the energy deposit in the strip with the minimal value between the first and second maximum ($\Delta E = E^{max2} - E^{min}$) has to be high enough.

- Total width in a window $\Delta\eta \times \Delta\phi = 0.0625 \times 0.2$ in the first em sampling. The width is calculated using the energy weighted sum $\omega_{tot1} = \sqrt{\sum E_i \cdot (i - i_{max})^2 / \sum E_i}$ where i is the strip number and i_{max} is the strip where the first maximum is located.

- Fraction of energy outside the shower core η in the first em compartment ($(E(\pm 3) - E(\pm 1))/E(\pm 1)$). Adding two ϕ-bins the ratio of the difference of the energy deposit in ± 3 and ± 1 strips around the strip with highest energy divided by the energy in ± 1 strips is calculated.

- Shower width using three strips ($\omega_{3\text{strips}}$) in the first em compartment. Using the highest energetic strip and its neighbour on each side the shower width is calculated by $\omega_{3strips} = \sqrt{\sum E_i \cdot (i - i_{max})^2 / \sum E_i}$ where i is the strip number and i_{max} is the strip where the first maximum is found. This width is a function of the shower position inside the cell. Like in the case of the width in the second sampling this effect is unfolded.

No isolation is required in a region around the core. γ/jet separation can be further improved by subdividing photons in two samples: converted photons and non-converted photons. In ATLAS around 25% of all photons convert in the material of the inner detector in a region of $R < 80$ cm and $|z| < 280$ cm where they can be efficiently identified. To reconstruct the tracks from a converted photon, there are two algorithms available. The first one reconstructs the tracks of 'early' conversions ($R < 40$ cm) and uses the information of the whole inner detector. The second one tries to reconstruct tracks using only the TRT ($40 < R < 80$ cm). Combining calorimeter and track information the following criteria can be used for γ/jet separation:

- the calorimeter cuts are optimised separately for converted and non-converted photons.
- for a reconstructed converted photon its momentum must be higher than a certain fraction of the cluster E_T. This criteria is only applied at low luminosity.
- in case no conversion is reconstructed a track veto of $p_T(thresh) = 5$ GeV is applied.

Details on photon identification are described in detail in [8].

The 'standard' photon identification cuts are optimised for a 80% photon efficiency for photons coming from Higgs decays. They are optimised in different rapidity and E_T regions. In rapidity there are two regions in the barrel ($|\eta| < 0.75, 0.75 < |\eta| < 1.37$) and three regions in the end-cap ($1.52 < |\eta| < 1.8, 1.8 < |\eta| < 2.0, 2.0 < |\eta| < 2.47$). The regions in the end-cap correspond to the regions with different granularity in the first sampling. In E_T different E_T bins were considered, namely 17–23 GeV, 25–35 GeV, 37–43 GeV, and 45–55 GeV. In the following, these set of cuts will be referred to as 'standard' photon identification cuts. For a 80% photon efficiency a γ/jet separation power of 1440 (880) was obtained at low (high) luminosity for photons with $E_T \approx 20$ GeV. These rates are normalised to the total number of jets in a certain energy range reconstructed using the fast detector simulation program ATLFAST [14]. Only QCD di-jet events are considered to calculate the jet rejection. Prompt photon, $W \to e\nu$, and $Z \to ee$ events are removed from the jet sample and the whole sample is suitably renormalised.

4 Photon Isolation

In the traditional approach an isolation cone with radius $R_0 = \sqrt{\Delta\eta^2 + \Delta\phi^2}$ is drawn around the photon direction. The energy found in this cone must be inferior to a certain fraction (ϵ_F) of the transverse photon energy.

$$E_T^{\text{isol}} < \epsilon_F \cdot E_T^{\gamma}$$

This cone approach can be modified by looking at all isolation cones with radius R with $R < R_0$ [15]:

$$E_T^{\text{isol}}(R) < \epsilon_S \cdot E_T^{\gamma} \cdot \left(\frac{1 - \cos R}{1 - \cos R_0}\right)^n$$

In this way the isolation criteria is implemented in a 'smooth' way. Hadrons are allowed within the isolation cone but they are required to be softer the closer they are to the photon axis. Theoretically, this 'smooth' isolation is preferred because it allows to define an isolated-photon cross section that does not depend on the fragmentation contribution. Direct photons will pass this isolation criteria whereas photons from bremsstrahlung and $\pi^0 \rightarrow \gamma\gamma$ are rejected. In a 'real' environment like ATLAS the situation is more complicated:

- The calorimeter readout has a certain granularity. In addition to the signal also contributions from electronic and pile-up noise have to be considered.
- A shower has a certain size which is around $R_{\text{min}} = 0.1$. Hence, the isolation cone cannot be a 'real' cone but more likely a ring, with a certain inner radius.
- some 'loose' isolation cuts are applied on LVL1 [9]. This cut has to be maintained because it is needed to reduce the rate to an acceptable level. There is a cut on $E_T(em)$ and $E_T(had)$ in a window of $\Delta\eta \times \Delta\phi = 0.4 \times 0.4$ around the core of 0.2×0.2 in the em calorimeter. Due to this isolation some of the prompt photons will be already rejected.
- Photons need to be reconstructed. The photon identification cuts are optimised to be 80% efficient independent of E_T for photons from $H \rightarrow \gamma\gamma$ events.

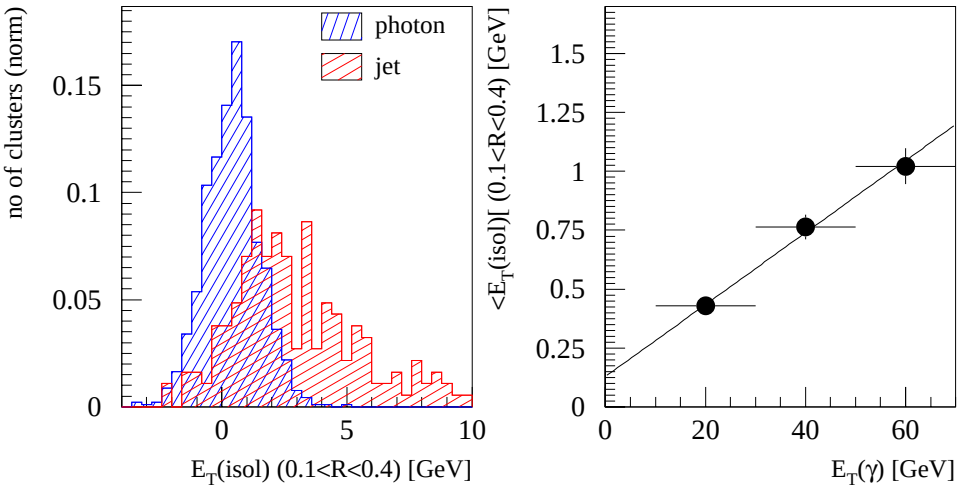

Figure 1: (a) Transverse energy deposit in an isolation ring of size $0.1 < R < 0.4$ for single photons and jets with $E_T \approx 20$ GeV. (b) E_T in the isolation ring $0.1 < R < 0.4$ as a function of the photon E_T. Both figures are shown for the low luminosity scenario.

Figure 1a shows as an example the energy deposit of single photons and jets with $E_T \approx 20$ GeV in an isolation ring with $0.1 < R < 0.4$. The isolation is shown for photons and jets after the trigger cuts and photon identification cuts. It can be seen that in the case of jets the transverse energy in the isolation ring is bigger than for photons. Figure 1b shows the scaling of the isolation with the

transverse energy of single photons.

In the following the gain in jet rejection will be studied using these two different isolation criteria for QCD prompt photons.

5 Comparison of the different Photon Isolation Methods

In this section the two different isolation methods described in the previous section will be compared. The possible gain in the γ/jet separation power after the 'standard' photon identification cuts will be estimated by tuning the isolation cuts in such a way that 99% of the prompt photons which have passed the 'standard' photon identification cuts survive the isolation criteria. In order not to loose too many photons the additional loss of photons after the 'standard' photon identification cuts was chosen to be 1%. Cross-checks with a 98% and 95% efficiencies show the same behaviour of the jet rejections for the different isolation methods and will not been shown in the following. A tuning of this sample proved to be very difficult due to a lack of statistics. Therefore, the optimisation is done using single photons with $E_T = 20, 40,$ and 60 GeV. The so obtained results are cross-checked with the prompt photon sample to verify they are well isolated.

Cuts	$\epsilon(\gamma_d)$ (%) $E_T > 17$GeV	$\epsilon(\gamma_b)$ (%) $E_T > 17$GeV	Rej jets $E_T \approx 20$GeV	$\epsilon(\gamma_d)$ (%) $E_T > 37$GeV	$\epsilon(\gamma_b)$ (%) $E_T > 37$GeV	Rej jets $E_T \approx 40$GeV
LVL1	90.8	75.0	110	100.0	82.7	190 ± 10
LVL2	87.9	67.5	610 ± 30	97.1	74.3	1000 ± 70
photon ID	73.0	50.0	1440 ± 110	84.3	58.8	2530 ± 280
$0.1 < R < 0.2$	73.0	46.9	2040 ± 170	84.3	45.2	2660 ± 310
$0.1 < R < .25$	73.0	47.4	2140 ± 190	84.3	44.8	2740 ± 320
$0.1 < R < 0.3$	73.0	46.9	2260 ± 210	83.7	44.5	2850 ± 340
$0.1 < R < .35$	72.3	44.7	2490 ± 240	83.7	45.2	2850 ± 340
$0.1 < R < 0.4$	72.3	45.6	2490 ± 240	83.7	41.5	2810 ± 330
$.15 < R < 0.4$	71.6	44.7	2280 ± 210	83.7	41.9	2770 ± 330
LVL1	90.8	75.0	110	100.0	82.7	190 ± 10
$0.1 < R < 0.4$	88.9	58.3	470 ± 20	98.8	54.8	520 ± 20

Table 1: Effect of different sets of isolation cuts on the efficiencies of prompt photons (γ_d) and photons from bremsstrahlung (γ_b). In addition, the corresponding jet rejections at $E_T \approx 20$ GeV and $E_T \approx 40$ GeV are given. The efficiencies and rates for the isolation algorithm are given after the trigger and photon identification cuts. For the isolation cone $0.1 < R < 0.4$ the rejections are as well given after the LVL1 cuts.

To study the effect of isolation with the traditional cone approach, cone sizes between R=0.2 and

R=0.4 were considered. Within the isolation ring the energy of all cells in the electro-magnetic and hadronic calorimeters were summed. The fraction of the photon energy in the isolation ring was varied to find the best performance in jet rejection. Table 1 shows the jet rejection for jets with $E_T \approx 20$ and 40 GeV and the impact of the isolation cuts on the prompt photons which is a sub-sample of the jet production. As seen in table 1 the jet rejection improves with increasing isolation cones and the best jet rejection is obtained for the cone size of R=0.35 or R=0.4 where due to the isolation cut an additional jet rejection of 70 (10)% is found for jets with $E_T \approx$20 (40) GeV at low luminosity. This is also visible in figure 2 which shows the background rejection as a function of E_T. The dip in the rejection at $E_T \approx 60$ GeV comes from LVL1. No isolation is required at LVL1 for showers having $E_T > 60$ GeV. Even after the fixed cone isolation cut this dip remains which indicate that the Level-1 isolation cut is stricter than the fixed cone isolation cut. To give an idea about the correlations between isolation cuts and the photon identification cuts the jet rejection after the LVL1 and the isolation cuts are as well shown in table 1 for different cone sizes.

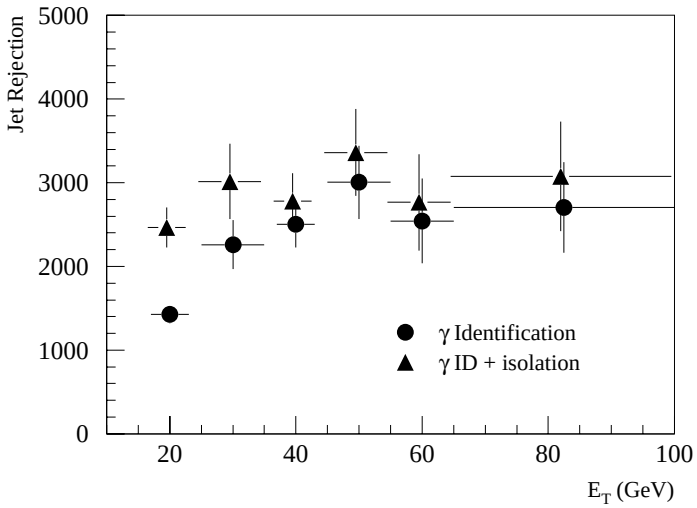

Figure 2: Jet rejection after photon identification and isolation cuts as a function of the jet E_T at low luminosity.

In the case of the modified cone approach ϵ_S as well as n were varied. Isolation cones were drawn around the core of $R_{\min} = 0.15$ in steps of 0.05 up to a maximal cone of $R_0 = 0.4$. The results are shown in table 2 which show a similar behaviour as obtained using fixed isolation rings. The best jet rejection is obtained for a maximal cone size of R=0.4. The rejection for different optimisation points of the smooth cone algorithm are given in table 3 for an outer cone size of R=0.4. It can be seen that a low value of n is preferred. For n$\rightarrow$ 0, the smooth cone approach converges towards the fixed cone approach. This indicates the smooth cone approach is not favoured as expected by theory. In Figure 3 the isolation is shown for cone sizes R=0.2 and R=0.4 for prompt photons after the full detector simulation and for the same showers on generator level. A clear E_T dependence for the isolation is found for the prompt photon sample after full simulation. This E_T behaviour is much less pronounced on generator level. This indicates the main component of the scaling

Cuts	$\epsilon(\gamma_d)$ (%) $E_T > 17$GeV	$\epsilon(\gamma_b)$ (%) $E_T > 17$GeV	Rej jets $E_T \approx 20$GeV	$\epsilon(\gamma_d)$ (%) $E_T > 37$GeV	$\epsilon(\gamma_b)$ (%) $E_T > 37$GeV	Rej jets $E_T \approx 40$GeV
photon ID	73.0	50.0	1440 ± 110	84.3	58.8	2530 ± 280
$0.1 < R < 0.2$	73.0	46.9	2030 ± 170	84.3	45.2	2630 ± 300
$0.1 < R < 0.3$	73.0	46.9	2250 ± 210	84.3	44.5	2810 ± 330
$0.1 < R < 0.4$	73.0	46.9	2300 ± 200	83.7	45.2	2810 ± 330

Table 2: Effect of isolation cuts on efficiencies of prompt photons and γ's from bremsstrahlung at low luminosity. In addition, the corresponding jet rejections at $E_T \approx 20$ GeV and $E_T \approx 40$ GeV are given.

n	ϵ_S	$R_{jet}(20$ GeV$)$	$R_{jet}(40$ GeV$)$
0.0	999.	2490 ± 240	2810 ± 330
0.1	0.175	2300 ± 200	2810 ± 330
0.25	0.195	2170 ± 190	2770 ± 300
0.5	0.26	2030 ± 170	2660 ± 310
1.0	0.70	1590 ± 120	2560 ± 290
1.5	1.85	1550 ± 120	2560 ± 290

Table 3: Jet rejection of 20 and 40 GeV jets at low luminosity after the trigger cuts and photon identification for different optimisations for the 'smooth' isolation method.

with E_T arises from the width of a shower in the calorimeter. Due to the shaping function the transverse energy in the isolation ring might become negative. Therefore, though the smooth cone approach is favoured by theory due to the distribution of soft particles around an isolated photon in the ATLAS detector this effect will be shaded by the photon shower size in the calorimeter and thus this method does not yield in a better performance compared to the fixed cone approach.

Table 1 shows the jet rejections and efficiencies obtained with the different isolation methods after the photon identification cuts as well as after the LVL1 selection. In the case of photons only a very small correllation is found between the isolation cuts and the photon identification cuts. Jets are broader and frequently accompanied by a small jet around. Therefore, the correllation is bigger.

Furthermore, it was investigated if an improvement in jet rejection can be obtained by applying the isolation separately in the em and the hadronic calorimeters. It is found that the performance is slightly degraded (by a few percent) for both isolation methods.

At high luminosity the situation is getting worse due to pileup. At the main bunch crossing 24 minimum bias events are added on average in the calorimeter and many more pile-up events come from other bunchcrossings which are partly seen in the calorimeters. These events overlap with the soft particles around the photon cluster. Therefore, a decrease of the γ/jet separation power is

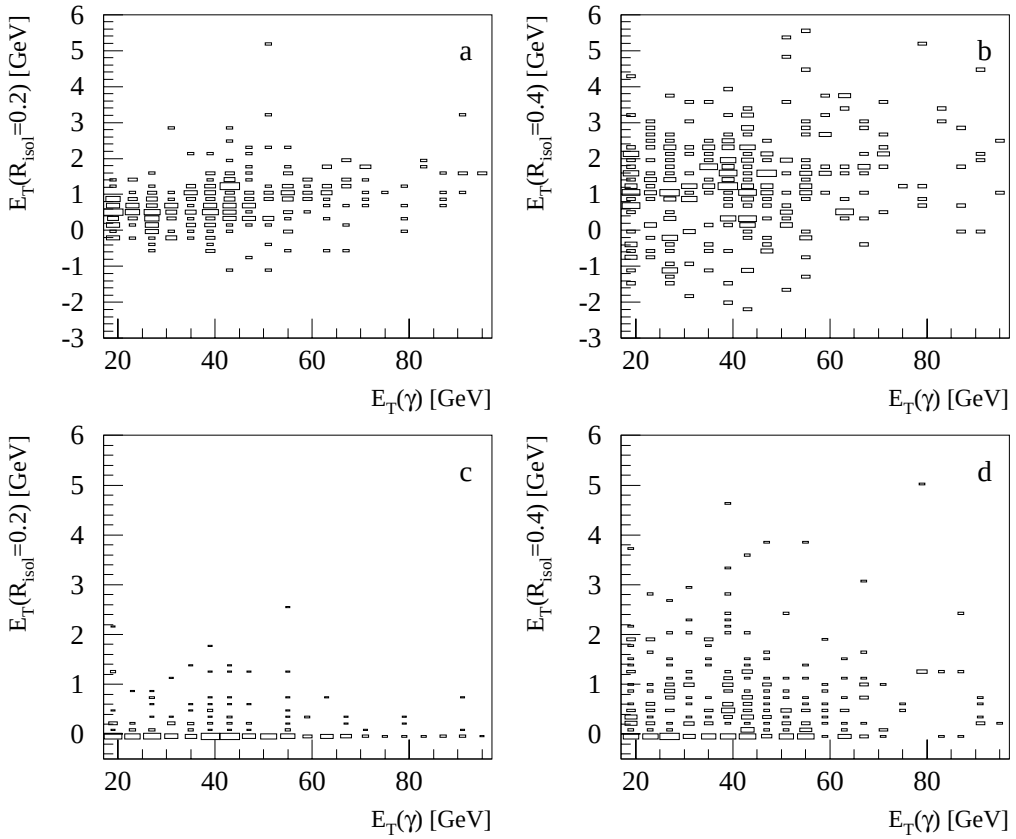

Figure 3: Isolation in different cones as a function of the photon E_T for prompt photons. The reconstructed isolation is shown (a) after the Level-1 trigger cuts and (b) after the trigger and 'standard' photon identification cuts. The corresponding isolation of these photons on the generator level are given in (c) and (d) respectively.

expected. Figure 4 shows the isolation in different cones as a function of the photon E_T. It can be seen that the E_T in the different isolation cones are typically larger than at low luminosity and the fluctuations are bigger. Looking at the average isolation E_T found in the ring around a cluster the scaling of the isolation energy with the cluster E_T is overshadowed by the pile-up effect. Applying 'zero suppression' helps to eliminate particles coming from the pile-up but will also eliminate soft particles around the photon. These effects will be studied in the following.

As for the low luminosity scenario, the parameters for isolation were tuned using single photon and cross-checked by the prompt photons found in the jet sample. Again the tuning was done for different cone sizes using the fixed and the smooth cone approach. Scenarios with and without zero-suppression at cell level have been studied. In the case of zero-suppression a noise cut of 2 and 6 times the sigma of the electronic noise level has been considered. Note, a better approach would be to cut on the sigma of the pileup and electronic noise contribution together, but unfortunately

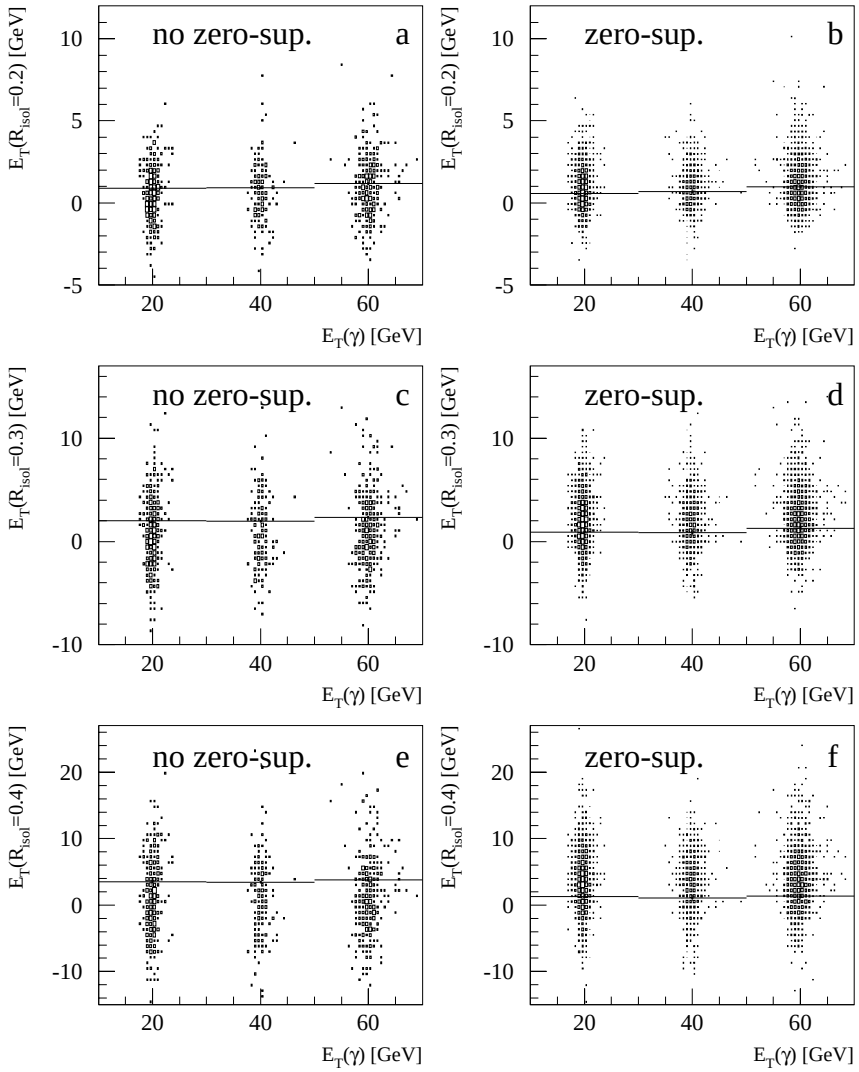

Figure 4: Sum of E_T in different isolation rings as a function of the photon E_T for single photons after the 'loose' level-1 trigger cuts at design luminosity. On the left sides the isolation is shown in case no zero-suppression applied at the cell level. The right sides shows the same figure but with zero-suppression applied. A symmetric cut of 2 times the sigma of the electronic noise was used. In addition to the isolation energy in the ring around the photon cluster the average isolation E_T is indicated.

method	R_{min}	R_{max}	n	ϵ	$\epsilon(\gamma)(\%)$	R_{jet} (20 GeV)
no	–	–	–	–	64.0	880
fixed	0.1	0.2	–	0.23	64.0	1020 (1.16)
smooth	0.1	0.2	0.1	0.23	64.0	1030 (1.17)
fixed	0.1	0.3	–	0.46	64.0	1040 (1.18)
smooth	0.1	0.3	0.5	0.46	64.0	1060 (1.21)
fixed	0.1	0.4	–	0.76	64.0	1040 (1.18)
smooth	0.1	0.4	1.0	0.60	64.0	1060 (1.20)

Table 4: Jet rejection of 20 GeV jets after the trigger cuts and photon identification for different optimisations for the fixed and smooth isolation method at high luminosity. No zero-suppression at cell level is applied.

method	R_{min}	R_{max}	n	ϵ	$\epsilon(\gamma)(\%)$	R_{jet} (20 GeV)
no	–	–	–	–	64.0	880
fixed	0.1	0.2	–	0.21	63.3	1010 (1.14)
smooth	0.1	0.2	1.5	0.27	63.3	1050 (1.20)
fixed	0.1	0.3	–	0.44	63.3	1040 (1.19)
smooth	0.1	0.3	1.5	0.92	63.3	1060 (1.21)
fixed	0.1	0.4	–	0.80	63.3	970 (1.11)
smooth	0.1	0.4	1.5	2.16	63.3	1060 (1.21)

Table 5: Jet rejection of 20 GeV jets after the trigger cuts and photon identification for different optimisations for the fixed and smooth isolation method at high luminosity. A symmetric two sigma cut in terms of the electronic noise at cell level is applied. See text for more information about how the jet rejection is calculated.

to date these values are not available in the 'standard' reconstruction program. As a 'rough' reference, depending on rapidity the pile-up contribution is around 2-3 times bigger than the electronic noise contribution [2]. Thus, a six sigma cut of the electronic noise contribution at high luminosity corresponds roughly to a two sigma cut at low luminosity. Using the energy calibration as obtained without any zero-suppression, a two (six) sigma cut changes the reconstructed transverse energies by 0.5% (3%) towards lower energies. Finding the best jet rejection for a 99% photon efficiency yields in better jet rejections in case a two sigma cut on the electronic noise at cell level is applied. Therefore, in the following, only results for a two sigma cut are shown. Applying this cut will affect slightly the shower shapes and thus the 'standard' photon identification cuts, which will not be adjusted any more for a 80% efficiency. To avoid retuning the cuts, at n-tuple level the 'zero-suppressed' clusters were matched with the 'non-zero-suppressed' clusters and its photon identification flag overwritten by the one from the 'non-zero-suppressed' cluster. Like this zero-suppression 'only' acts on the cells within the isolation ring.

Table 4 shows the results in case no zero-suppression is applied at the cell level. Table 5 summarises the results in case a symmetric cut of two times the sigma of the electronic noise level is used. The best jet rejection is achieved for a cone size of $R = 0.3$. Due to the pileup effects a smaller isolation cone is preferred than at low luminosity. The jet rejection obtained with the smooth cone algorithm yields in slightly better jet rejections compared to the fixed cone algorithm. No improvement nor degradation of the γ/jet separation power is observed if zero-suppression is applied. This result does not exclude a possible improvement if zero-suppression is applied. As mentioned earlier, a more correct way to apply zero-suppression is to cut on the sigma of the pileup and electronic noise contribution. In the high luminosity case the gain in rejection after the photon identification cut is around 15-20% at around 20 GeV and negligible for $E_T > 40$ GeV.

At high luminosity no gain in jet rejection is found for higher values of the photon E_T. At low luminosity the improvement in jet rejection is smaller at high E_T values compared to $E_T \approx 20$ GeV. As seen in figure 4, a simple scaling of the energy in the isolation ring around a photon cluster is not optimal and a combination of the scaling and a constant term is more adequate. In the following, the isolation energy will be parametrised in the form $E_T(isol) = a + b \cdot E_T(\gamma)$. No attempt is made to add a constant term to the smooth cone approach, because of the very similar results. However, the smooth cone isolation might be modified by

$$E_T^{\mathrm{isol}}(R) < \epsilon_S \cdot E_T^{\gamma} \cdot \left(\frac{1-\cos R}{1-\cos R_0}\right)^n + a(R)$$

where a(R) is the constant term which will be dependent on the outer cone radius. It will increase for larger cone sizes. In this case, the determination of the parameters of this isolation method is no longer trivial. In addition, it is not clear that such an approach still fulfills the original theoretical considerations, because this constant term arises purely from experimental aspects such as electronic and pile-up noise.

For the 'modified' cone approach, where the parametrisation is parametrised as $E_T(isol) = a + b \cdot E_T(\gamma)$, the optimal isolation rings as found for the fixed cone isolation are used at low and high luminosity. At high luminosity the tuning is done once using zero-suppression and once without. The so obtained jet rejections are shown in figure 5 and figure 6 for low and high luminosity respectively. Comparing the jet rejections obtained with and without zero-suppression,

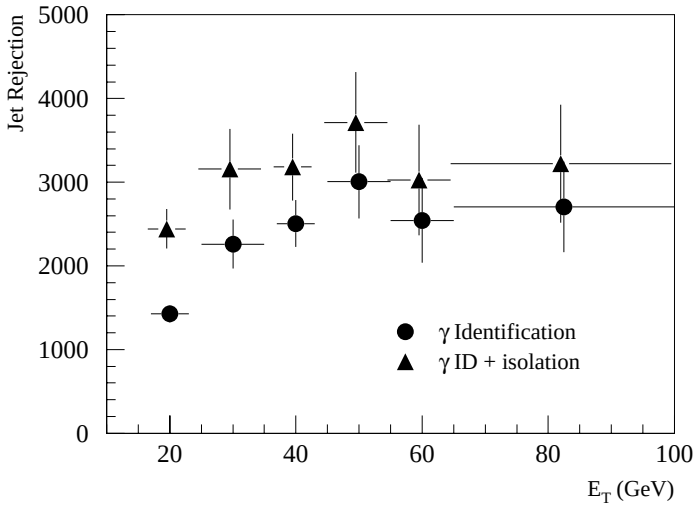

Figure 5: Jet rejection after photon identification and isolation cuts as a function of the jet E_T at low luminosity. The E_T found in the isolation ring of size $0.1 < R < 0.4$ is parametrised in the form $E_T(isol) = a + b \cdot E_T(\gamma)$

nearly the same values are found for photons with $E_T \approx 20$ GeV, both at low and high luminosity. At low luminosity, the jet rejection for high-E_T photon candidates increases from 10% using the 'simple' fixed cone algorithms to 20%. At high luminosity the improvement lies only of the order of few percent, both with or without applying zero suppression.

Depending on the analysis or for crosschecks a cleaner photon sample might be obtained by applying stricter isolation cuts, while accepting lower photon efficiencies. Note, that tightening the 'standard' photon identification cuts would result in a worse performance. These cuts are already tuned in such a way that a further tightening would cut hard in the distributions. On the other hand the distribution of the isolation criteria is much smoother (see figure 1a). To give an idea, the gain in jet rejection for different photon efficiencies is shown in table 6 and 7 for low and design luminosity respectively. As an example a further jet rejection by a factor of two would imply an isolation cut, which rejects an additional 10% (20%) of prompt photons after the standard photon identification cuts at low (high) luminosity.

6 Photon Isolation for Photons from $H \rightarrow \gamma\gamma$ decays

The study presented in the last section will be now extended to photons from $H \rightarrow \gamma\gamma$ decays. As shown in the previous section, the best jet rejection is achieved using a parametrisation for the transverse energy deposit in the isolation ring of the form $E_T(\text{isol}) = a + b \cdot E_T(\gamma)$. Thus this parametrisation will be used in the following. Note, that due to the different 'physics signature' the isolation requirements are not necessarily the same as the ones for prompt photons. In order to achieve the best possible jet rejection all photon identification cuts were tuned together with

cut	$R_{jet} \approx 20$ GeV	$R_{jet} \approx 40$ GeV
γ identification	1440	2530
+ isolation (99%)	2470 (1.72)	3210 (1.27)
+ isolation (95%)	2660 (1.85)	4130 (1.63)
+ isolation (90%)	3320 (2.31	4820 (1.91)
+ isolation (80%)	3900 (2.72)	5630 (2.23)
+ isolation (50%)	7920 (5.51)	8800 (3.48)

Table 6: Jet rejections of 20 GeV and 40 GeV jets after the trigger cuts and photon identification for different isolation criteria at low luminosity. The jet rejections are shown for isolation cuts which keep at least 99, 95, 90, 80% of single or prompt photons after the 'standard' photon identification cuts. The values in parenthesis are the relative rejections with respect to the trigger and photon identification cuts.

cut	no zero-suppression	with zero-suppression
γ identification	880	880
+ isolation (99%)	$1030 \pm 70(1.17)$	$1030 \pm 70(1.17)$
+ isolation (95%)	$1210 \pm 90(1.38)$	$1130 \pm 80(1.28)$
+ isolation (90%)	$1430 \pm 110(1.62)$	$1240 \pm 90(1.42)$
+ isolation (80%)	$1720 \pm 150(1.96)$	$1430 \pm 110(1.63)$
+ isolation (50%)	$3470 \pm 440(3.95)$	$3110 \pm 360(3.54)$

Table 7: Jet rejections of 20 GeV jets after the trigger cuts and photon identification for different isolation criteria at high luminosity. The jet rejections are shown for isolation cuts which keep at least 99, 95, 90, 80% of single or prompt photons after the 'standard' photon identification cuts. The values in parenthesis are the relative rejections with respect to the trigger and photon identification cuts. Results are shown without using zero-suppression and for a symmetric 2σ cut on the electronic noise contribution at cell level.

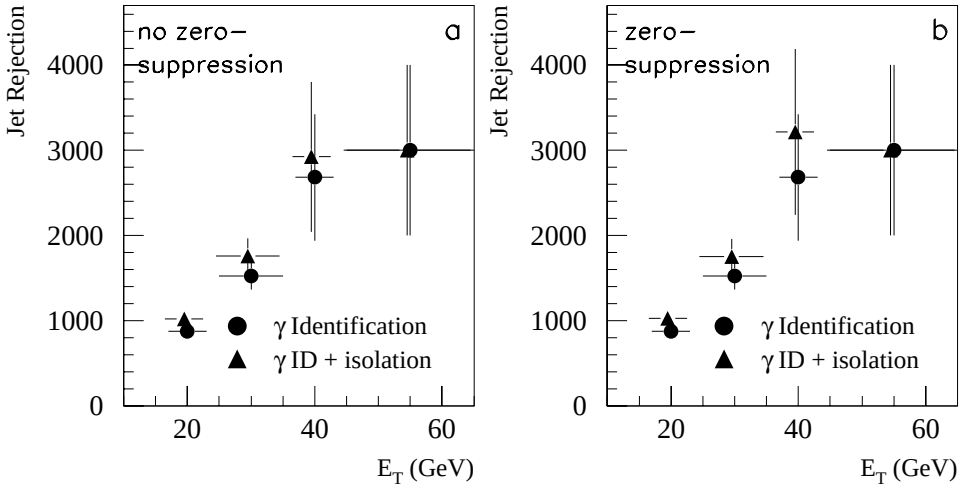

Figure 6: Jet rejection after photon identification and isolation cuts as a function of the jet E_T at design luminosity. The distributions are shown in case (a) no zero-suppression is applied and (b) in case a symmetric cut of two times the sigma of the electronic noise contribution is applied. The E_T found in the isolation ring of size $0.1 < R < 0.4$ is parametrised in the form $E_T(isol) = a + b \cdot E_T(\gamma)$

the isolation criteria for 80% photon efficiency. The results are shown in figures 7 and 8 for low and design luminosity respectively. At low luminosity the jet rejection is higher by 40% (30%) compared to the standard photon identification cuts, which were as well tuned for 80% photon efficiency. Compared to the results for the jet rejections obtained for prompt photons at low luminosity (see tables 6 and 7), the improvement in jet rejection is less at $E_T \approx 20$ GeV and bigger at higher transverse energies. Note that for prompt photons the final photon efficiency is due to the tuning less than 80%. At high luminosity the tunings were again done for the cases that no zero suppression is applied and for the case of a symmetric two sigma cut of the electronic noise at cell level. Contrary to what was done for the analysis of prompt photons, two separate tunings were done for the photon identification cuts together with the isolation criteria. As shown in [8] no improvement in the jet rejection is achieved in case zero suppression is applied for the standard photon identification cuts.

An additional jet rejection of 10% is found in case zero suppression is not applied and 20% in case zero suppression is applied. Contrary to the results found for prompt photons, a better jet rejection is achieved, in case zero suppression on cell level is used. The thus obtained photon efficiencies as a function of rapidity are shown in figure 9 for low and design luminosity. The photons efficiencies are around 80% for all rapidities, with a dip in the barrel/end-cap region and toward the end of the electro-magnetic calorimeter. The figure shows as well that the photon identification cuts cut hard on conversions especially in the barrel regions.

In this study the isolation criterium have not been varied as a function of rapidity. Due to the different amount of material in front of the calorimeter for different rapidities and due to the fact

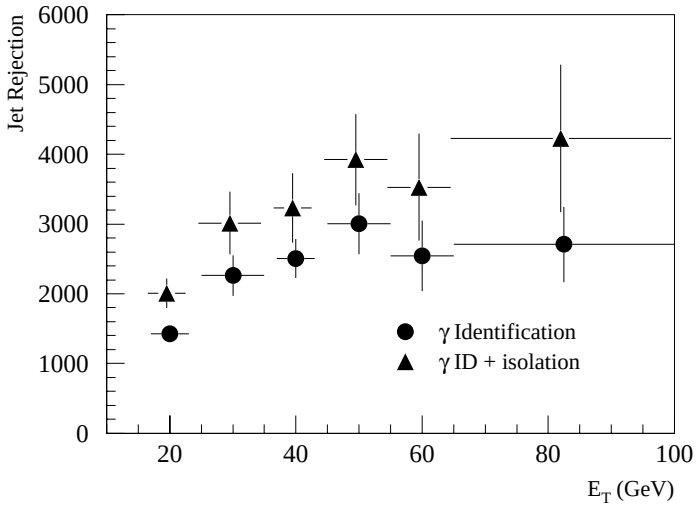

Figure 7: Jet rejection after photon identification and isolation cuts as a function of the jet E_T at low luminosity. The tuning was done to achieve a 80% efficiency for photons coming from Higgs decays.

that the photon shower sizes scale with energy and not E_T, the leakage outside the shower core into the isolation ring varies with rapidity. Taking this effect into account might slightly improve the jet rejection. In addition, the isolation cuts might be tuned differently for converted and non-converted photons.

These results show that besides the shower shape analysis and isolation into the hadronic calorimeter the isolation around an electro-magnetic cluster is a useful quantity for γ/jet separation. Nevertheless, isolation cuts need to be very carefully applied. They cover a big region in the calorimeter and hence will be quite sensitive to pileup and electronic noise contributions, as well as to dead and noisy cells. In addition isolation is quite physics dependent and if applied as standard criteria on the event filter, they must be loose enough in order not to throw away physics. Probably they are better suited to be applied 'only' during the offline reconstruction.

7 Conclusions

γ/jet separation has been studied in detail in [8]. The standard photon identification cuts are mainly based on the shower shape analysis within the electro-magnetic calorimeter and the leakage into the first sampling of the hadronic calorimeter. Using these cut values which were optimised for a 80% photon efficiency (independent of E_T) for photons from $H \rightarrow \gamma\gamma$ decays, a jet rejection of 1440 (880) was found at low (high) luminosity. In this note the γ/jet separation power was studied for the case that in addition to the standard photon identification cuts as studied in the past an isolation around a photon candidate is added. For the case of prompt photons different isolation criteria have been studied. Firstly a 'simple' cone or better to say ring algorithm, which sums the E_T deposit in all cells in a ring around a photon candidate, with an inner cone size of

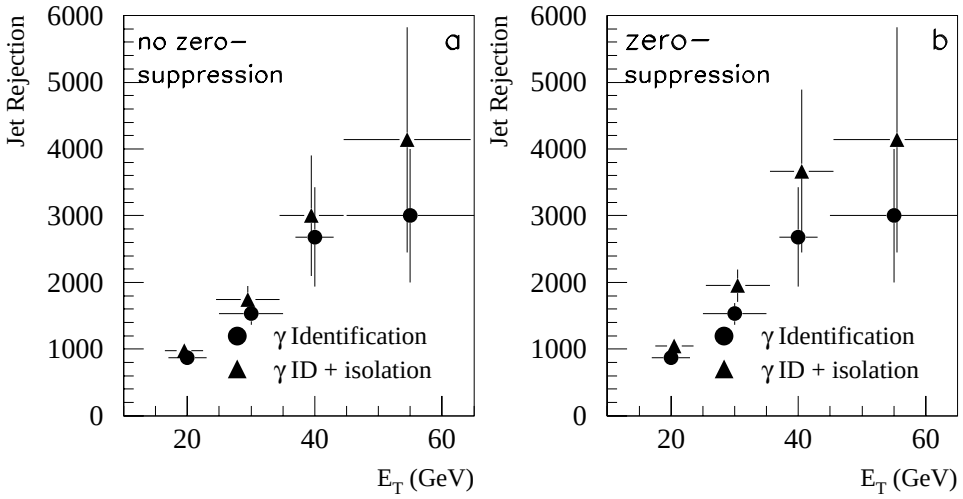

Figure 8: Jet rejection after photon identification and isolation cuts as a function of the jet E_T at high luminosity. The tuning was done to achieve a 80% efficiency for photons coming from Higgs decays. In (a) the jet rejections are shown in case no zero-suppression is applied at cell level, (b) shows the results in case a symmetric cut of two sigma of the electronic noise is applied.

around $R = 0.1$. This inner cone size is determined by the shower size of an electro-magnetic shower. The so found transverse energy must be less than a certain fraction of the photon E_T. In the smooth cone approach all isolation cones below a certain radius in the rapidity-phi space are considered and must be below a certain fraction (dependent on R) of the cluster E_T. This method allows a certain amount of hadrons within the isolation cones. Both method yield in very similar results in jet rejection at low as well as design luminosity. Compared to the 'fixed' cone approach, the smooth cone approach is more stable. It gives very similar jet rejections for whatever chosen outer cone size. Using isolation in addition to the standard photon identification cuts an improvement in the jet rejection of 70% (10%) for clusters with $E_T \approx 20$ (40) GeV at low luminosity. These results were obtained by accepting an addition loss of 1% in the photon efficiency. At high luminosity a γ/jet separation power of around 1100 is found for jets with $E_T \approx 20$ GeV. In the high-E_T range, the isolation criteria does not improve the jet rejection. To improve the jet rejection at high E_T values a third isolation method was chosen. The simple cone algorithm was modified and a constant term was added. Using this method, very similar jet rejections have been found compared to the other two methods at $E_T \approx 20$ GeV. At 40 GeV the γ/jet separation power improved by 20% at low luminosity compared to the 'standard' photon identification cuts. At high luminosity this method yields in an improvement of only few percent. The 'smooth' cone approach is favoured by theory and will 'ideally' keep prompt photons and reject photons from bremsstrahlung in the way isolation is implemented. However, in the ATLAS environment this advantage is overshadowed by the larger detector effects.

The cone approach modified by adding a constant term to the fixed cone algorithm yields in the best jet rejections for various E_T ranges. Using this method a new optimisation of the standard

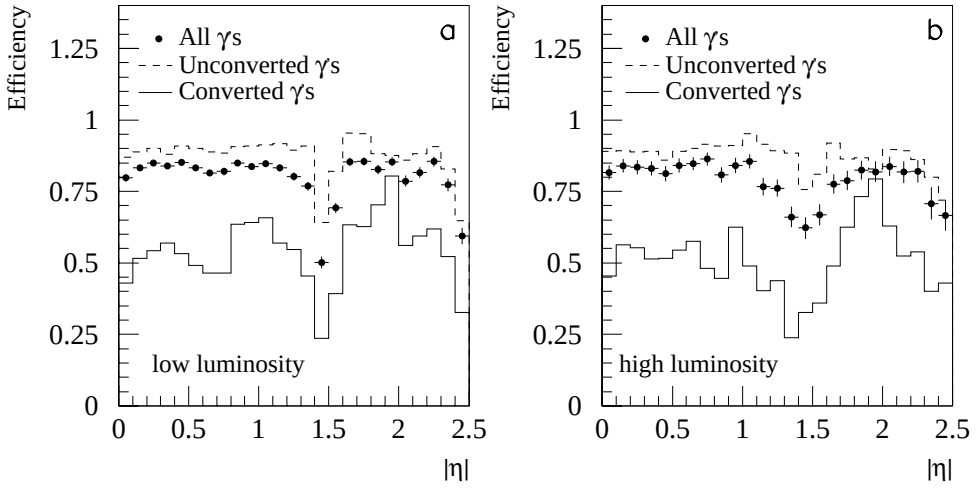

Figure 9: Efficiency as a function of rapidity for photons from Higgs days at (a) low luminosity and (b) design luminosity.

photon identification cuts together with the isolation criteria was done for a 80% efficiency for photons from $H \rightarrow \gamma\gamma$ decays. Compared to the previous tuning the jet rejection of 2030 (3260) was found at low luminosity for jets with $E_T \approx 20(40)$ GeV. At design luminosity a γ/jet separation power of 980 and 1050 is found for 20 GeV jets without and with zero-suppression applied. This corresponds to an improvement of 10-20%.

If isolation is used as one criteria for photon identification it needs to be applied very carefully. Isolation is physics dependent and hence if it would be applied on the event filter level, only a very loose isolation around a photon candidate should be applied. This might help in improving the jet rejection at low luminosity. At high luminosity however the gain is not very significant, so that in this case isolation should be only applied in the offline reconstruction of a specific physics process.

This study had a first look at photon isolation for prompt photons and photons from $H \rightarrow \gamma\gamma$ decays. The results presented just give a first indication because of the following shortcomings.

- The results in the case of prompt photons had to be done using single photons and been crosschecked by the available prompt photon sample. This is due to a lack of statistics in the prompt photon sample, which is a sub-sample of the jet production sample. In the future, dedicated prompt photon events should be simulated.

- The comparison of the fixed cone and smooth cone approach suffered from the fact that the jet/prompt photon events had to pass the 'loose' isolation cuts of the pseudo-LVL1 filter which might bias the results. Sofar, this has been necessary to obtain manageable datasets. For prompt photon studies an unbiased sample would be appreciated.

- This study was carried out using simulated events with an 'old' detector layout. Compared

to the actual layout less material in front of the calorimeters are present. In addition the gap between barrel and end-cap calorimeters will be enlarged by 4 cm, leading to a slightly non-pointing geometry in the end-cap and a slightly larger crack region, which will be unusable for photon identification.

- The effect of zero suppression at cell level on the energies in the isolation cones could not be studied correctly at high luminosity. To apply zero-suppression a symmetric cut was chosen which depends on the width of electronic noise contribution. At high luminosity a cut on the sigma of the sum of the electronic and the pileup noise contribution should be applied.

References

[1] ALEPH, DELPHI, L3 and OPAL Collaborations, LHWG-Note-2001-03, (2001)

[2] ATLAS collaboration, Calorimeter Technical Design Report, CERN/LHCC/96-41, ATLAS TDR 2, (1996)

[3] ATLAS collaboration, Inner Detector Technical Design Report, CERN/LHCC/97-17, ATLAS TDR 5, (1997)

[4] Offline Software Group, ATL-SOFT-95-011, (1995)

[5] ATLAS collaboration, ATLAS Detector and Physics Performance TDR, CERN/LHCC/99-14, ATLAS TDR 14, (1999)

[6] Application Software Group, CERN program library long writeup W5013.

[7] T. Sjöstrand, Comp. Phys. Comm. **82** (1994) 74;
T. Sjöstrand, Comp. Phys. Comm. **39** (1986) 347.

[8] M. Wielers, ATL-PHYS-99-016, (1999)

[9] http://atlasinfo.cern.ch/Atlas/GROUPS/DAQTRIG/SIMULATION/software/atman.html#Atrig-Manual

[10] A. Dell'Acqua et al., ATL-PHYS-97-102, (1997)

[11] ATLAS collaboration, Trigger Performance Status Report, CERN/LHCC/98-11, (1998)

[12] Offline Software Group, ATL-SOFT-94-015, (1994)

[13] J. Schwindling, 'The reconstruction code for the electromagnetic calorimeter in ATRECON', http://atlasinfo.cern.ch/Atlas/GROUPS/PHYSICS/EGAMMA/emreco973.ps (1997)

[14] E. Richter-Was et al., ATL-PHYS-98-131, (1998)

[15] S. Frixione, Phys. Lett. **B429** (1998) 369;
S. Frixione, hep-ph/9809397 (1998)